Optimized acousto-optic modulation for the *V*-type electromagnetically induced transparency in rubidium-87 D_1 line

[1, 2] Dastan Khalid and [1]Hawri O. Majeed

[1] Department of Physics, College of Education, Old Campus, University of Sulaimani, Sulaimani, Iraq, P. O. Box 334, dastan.khalid@univsul.edu.iq
[2] Department of Physics and Astronomy, University of Leeds, Leeds, UK, LS2 9JT

Received: 19.03.2017

Abstract. We present an experimental setup of optimized acousto-optic modulator designed for observing a *V*-type electromagnetically induced transparency resonance in the D_1 line of rubidium-87, with the full width at half maximum being equal to 2.7 MHz. Possible artefacts and undesirable influences on the signal resulting from this method are discussed in detail. The solutions to such technical challenges as beam steering and intensity fluctuations are found in optimization of optical setup. The reported method offers a number of advantages such a single external-cavity diode laser to create a bichromatic optical field outside the laser, whereby both the coupling and probe beams have identical properties. Moreover, the both beams are equally affected by environmental perturbations to the laser. Subsequently, the influence of mode hopping, beam-power fluctuation and frequency drift on the resonance can be eliminated. This negates a need in complicated and expensive temperature and current stabilizations, as well as in a locking unit. The simplicity and stability of the improved setup make our method suitable for many applications based upon electromagnetically induced transparency, especially those in the field of precision measurements.

Keywords: electromagnetically induced transparency, acousto-optic modulation, coherent control of atomic interactions with photons.

PACS: 42.50.Gy, 42.60.Fc, 42.79.Jq, 32.80.Qk
UDC: 534.42, 535.3

1. Introduction

Electromagnetically induced transparency (EIT) results from destructive quantum interference among different excitation pathways in an atomic ensemble (see Fig. 1). A peculiar characteristic of the EIT is enhancement of optical transmission of a weak probe beam due to the presence of a strong coupling beam. This increase in the transmission might suggest saturation due to optical pumping. However, the phenomenon occurs fundamentally when the coupling beam causes Stark splitting of the excited state. In its turn, this creates the two absorption paths for the weak probe beam. Thus, the destructive interference between these two absorption channels produces enhanced transmission, which is the essence of the EIT.

Due to this unique modification, the EIT technique has many applications such as, e.g., lasing without inversion [1], slow light [2], optical switches [3], quantum memory [4], quantum information processing [5] and sensitive magnetometry [6]. Detailed theoretical treatment and experimental realizations of the effect, along with further applications, can be found in the comprehensive topical reviews by J. P. Marangos [7] and M. Fleischhauer et al. [8].

There are different methods for producing the EIT effect. As an example, one can utilize two independent narrow-linewidth (usually~1 MHz) lasers [9–12], where one of the lasers is locked to

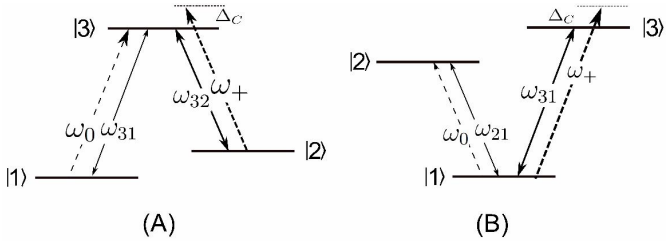

Fig. 1. Suitable atomic-energy configuration leading to observation of the EIT. Λ-type and *V*-type energy configurations are shown in panels (A) and (B), respectively. ω_{31}, ω_{21} and ω_{32} are respectively the energy differences between levels |3⟩ and |1⟩, |2⟩ and |1⟩, and |3⟩ and |2⟩. ω_+ and ω_0 denote respectively the coupling and probe optical fields, and Δ_c implies the coupling-beam detuning from ω_{31}.

a given transition and the other scans another transition. The other methods are based on a single laser and a modulation technique such as injection-current or external-phase modulators [13, 14].

In the case of small frequency detuning (≤ 40 MHz), a single laser and an acousto-optic modulator (AOM) can also be used to create the EIT signal [15]. However, the fundamentals of this approach depend on the parameters introducing certain artefacts to the observed signal. These artefacts result from fluctuations in the beam intensity and beam-steering effects, which impose undesirable variation in the Rabi frequency and a change in the degree of overlap between the coupling and probe beams. A degrading effect of these phenomena on the EIT resonance has earlier been found. To be more specific, these effects broaden and destroy the EIT resonance, as explained below.

Although AOMs have already been used for producing the EIT resonance, to the best of the authors' knowledge, there are no reports addressing technical challenges and intrinsic problems faced by this technique. This is especially crucial when the EIT is used in sensitive and high-precision measurements. The subject of this work is to discuss the above artefacts and problems, and to present the methods for stabilizing the intensity and governing the beam steering. To reach this aim, we optimize a robust optical setup in which the AOM is used to produce the EIT resonance. We consider the principles underlying our method in Section 2 and explain its essence in Section 3. The results are discussed in Section 4. Finally, we draw conclusions in Section 5.

2. Principles of the method

Observation of the EIT requires certain conditions to be met. Two of the most fundamental prerequisites related to the optical fields are availability of a bichromatic optical field and transformation of this bichromatic field into a resonant, strongly coupling beam and a weak scanning probe beam, or vice versa. There are also additional conditions related to the choice of atoms and atomic states, which are elucidated in Refs. [7, 8, 16]. The other requirements also related to the optical field include a rightly chosen polarization (when Zeeman sub-levels are used), a sufficient intensity, and coherence between the two beams. They will be discussed in the following sections.

The AOM should satisfy the both conditions mentioned above. The reason is that, among the other functions such as intensity modulation, beam steering, optical filtering and isolating [17], the AOM can also be operated as a frequency-shifting device. When used as a frequency modulator, the AOM performs the two main tasks. The first one is increasing or decreasing the frequency of the incident laser beam, which are referred to as up- or down-frequency shifts, respectively. The frequency change is dependent on the direction of the incident optical wave vector with respect to the acoustic wave vector.

The frequency shift mentioned above creates a bichromatic beam, which is one of the optical requirements for the EIT. The second requirement is met when the AOM produces a variable frequency shift, i.e. works as a scanner. Variable modulation occurs across a certain width defined by a manufacturer's design. To produce the scanning probe (or coupling) beam, the radio-frequency signal applied to the AOM is modulated by applying a triangular-waveform signal to an AOM driver. The amplitude of the signal applied changes the frequency-shift extent and, hence, the diffracted beam is characterized by a frequency range depending on this triangular waveform. This means that the amplitude of the signal applied controls the scanning width while the frequency of the waveform governs the scanning frequency.

3. Experimental methods

In our experiments, an external-cavity diode *laser* from Toptica DL100, with the wavelength of about 795 nm, is tuned to $5^2S_{1/2}: F = 2 \rightarrow 5^2P_{1/2}: F' = 1$ transition in ^{87}Rb. Since all of our observations and measurements have been carried out using ^{87}Rb atoms, the term '^{87}Rb' will be omitted hereafter. We have a *V*-type configuration when the laser beam is separated into two components using a polarizing beam splitter, as shown in Fig. 2. The *s*-polarized beam acting as a weak probe beam (ω_0) is directed at a reference cell that contains ^{85}Rb and ^{87}Rb atoms in natural abundances. The cell has the length 50 mm and the diameter 25 mm. It is housed in a three-layer μ-metal cylinder, for which the shielding factor of the measured magnetic field is larger than 10^4. The *p*-polarized beam serving as a strong coupling beam (ω_+) is directed onto the AOM.

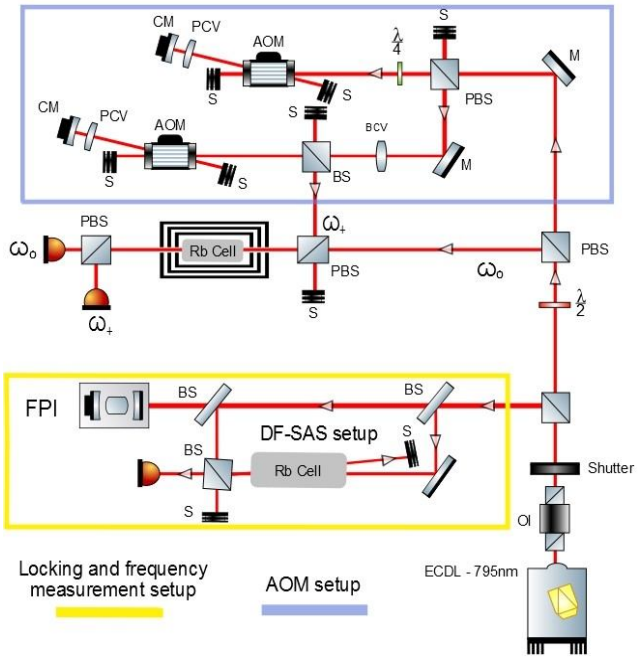

Fig. 2. Experimental setup built for achieving the EIT effect with AOM. Yellow block corresponds to frequency-measurement components which use a Doppler-free saturated absorption spectroscopy (DF-SAS) and a Fabry-Pérot interferometer (FPI). Light blue block corresponds to AOMs, where shifting and modulation of the optical field are implemented. The main experimental components are as follows: external-cavity diode laser (ECDL), optical isolator (OI), polarizing-beam splitter (PBS), plane mirror (M), beam stop (S), Bragg cell (AOM), planoconcave lens (PCV), concave mirror (CM), biconcave lens (BCV), beam splitter (BS), quarter-wave plate ($\lambda/4$) and half-wave plate ($\lambda/2$). The probe beam ω_0 is tuned to $5^2P_{1/2}: F' = 1$ and the coupling beam ω_+ is frequency-shifted by +814.5 MHz. The Rb-cell used for observing the EIT effect is placed in a three-layer μ-metal with the shielding factor of the measured magnetic field not less than 10^4.

Brimrose TEF-200-50-795 AOMs offer a central-frequency shift 200 MHz and the width 50 MHz at 795 nm. This gives the frequency-shifting abilities as large as 175–225 MHz, depending on the d.c. voltage applied to the AOM driver. For a single AOM in double-pass configuration, where a (plus or minus) first-order diffracted beam is retroreflected back to the AOM cell and a zero-order beam is blocked as shown in Fig. 2, the central-frequency shift +400 MHz is achievable. In this work, the two AOMs are set up in the double-pass configuration, where the frequency of the strong coupling beam ω_+ is chosen to be +814.5 MHz with respect to ω_0. This +814.5 MHz frequency difference between the two beams corresponds to the energy difference between the excited states $5^2P_{1/2}$: F' = 1 and F' = 2 (see Ref [18]). As a result, the excitations from $5^2S_{1/2}$: F = 2 transition form a V-type configuration. The two beams ω_0 and ω_+ are recombined through another polarizing-beam splitter, so that they co-propagate through the cell. This eliminates a Doppler-dependent signal.

As discussed previously, application of triangular waveform to the AOM driver modulates the radio-frequency signal at the AOM. As a result of this modulation, the frequency shift in the optical field also follows this triangular waveform. Software and hardware from the National Instrument have been used to generate and control the triangular waveform. This external signal is applied to one of the drivers. Nonetheless, the triangular signal could also be applied to the both drivers whenever higher scanning widths are required. A standard function generator can become an alternative to the computer-generated output voltage. However, we have chosen the former method in this work for the reasons of flexibility and ease of control.

4. Results and discussion

It is necessary to select a required frequency difference for the incident laser beam in order that ω_+ had the correct interacting frequency with respect to ω_0, as required for the V-type interaction. Initially the experiment has been arranged in a manner similar to that of Doppler-free saturated absorption spectroscopy (see Fig. 3). Here the two beams ω_0 and ω_+ are counter-propagating through the atomic ensemble and each of the beams is monitored separately. In this modification, the laser is scanned across the whole Rb spectrum and the result is compared with the reference data of the Doppler-free saturated absorption spectroscopy.

Since the coupling beam ω_+ has been shifted by +814.5 MHz, a saturation of F = 2 → F' = 1 occurs at the position F = 2 → F' = 2 (see Fig. 4). This is because, for the same atomic velocity group, the atoms 'see' one of the beams blue-shifted to the extent the F' = 1 coincides with the F' = 2 energy level. This result shows that the V-type EIT could in principle be obtained when the other conditions related to the EIT are met.

After the frequency of ω_+ has been set as required with respect to ω_0, the two beams are arranged in a co-propagating configuration through the interaction cell, as shown in Fig. 3. When the laser is tuned to F = 2 → F' = 1 and the AOM is detuned around F = 2 → F' = 2 due to application of the triangular waveform to the AOM driver, an EIT signal is observed (see Fig. 5). The EIT is found to have the full width at half maximum equal to 2.7 MHz.

There appear some technical difficulties when producing this signal, which must be obligatory solved if the EIT signal is to be used for highly precise measurements. These difficulties are related to the very working principle of the AOM. The first difficulty is a dependence of the diffraction angle and, therefore, of the modulation frequency on the radio-frequency signal applied to the AOM driver. Increasing voltage applied to the AOM driver increases the diffraction angle, and vice versa. Therefore, when the triangular waveform is applied

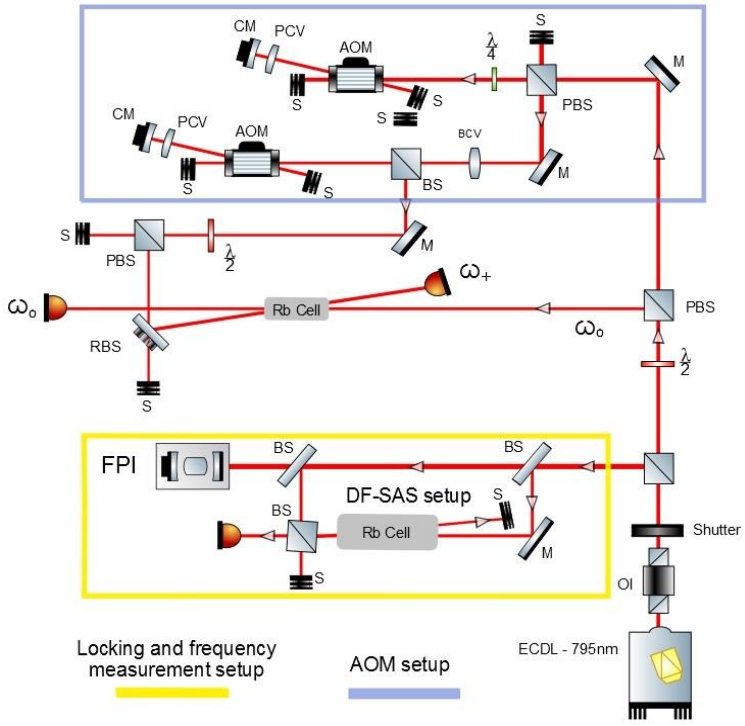

Fig. 3. Experimental setup for selecting a correct frequency ω_+. Counter-propagating ω_0 and ω_+ beams are monitored separately in different channels of an oscilloscope and the entire signal is compared with the reference signal obtained using Doppler-free saturated absorption spectroscopy. The experimental components are the same as in Fig. 2, except for an additional rotating beam splitter (RBS).

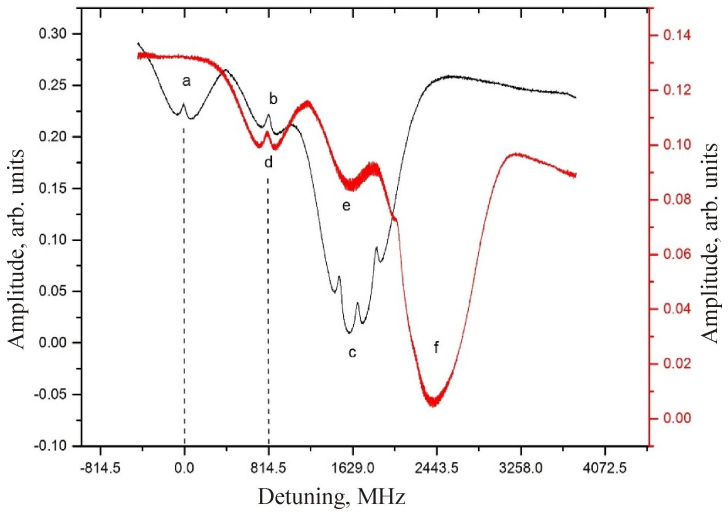

Fig. 4. Spectra of ^{85}Rb (F = 3) and ^{87}Rb (F = 2) transitions. Red line corresponds to Doppler-broadened spectrum of ^{85}Rb (F = 3) and ^{87}Rb (F = 2), and black line to Doppler-free saturated absorption spectrum of the same transitions obtained from the reference signal as a part of optical setup for stabilizing and locking. The peaks are as follows: (a) ^{87}Rb: F = 2 → F' = 1 hyperfine transition, (b) ^{87}Rb: F = 2 → F' = 2 hyperfine transition, (c) ^{85}Rb: F = 3 transition that reveals hyperfine levels F' = 2 and F' = 3, as well as crossover, and (d) ^{87}Rb: F = 2 → F' = 1 transition. Panels (e) and (f) show Doppler-broadened spectra of respectively ^{87}Rb: F = 2 → F' = 2 and ^{85}Rb: F = 3 transitions. The peak ^{87}Rb: F = 2 → F' = 1 is saturated by counter-propagating beam due to the frequency shift +814.5 MHz, as seen from panel (d). The latter is clearly seen when the two spectra are compared: saturation of ^{87}Rb: F = 2 → F' = 1 in the 'red' spectrum coincides with that of ^{87}Rb: F = 2 → F' = 2 in the 'black' spectrum.

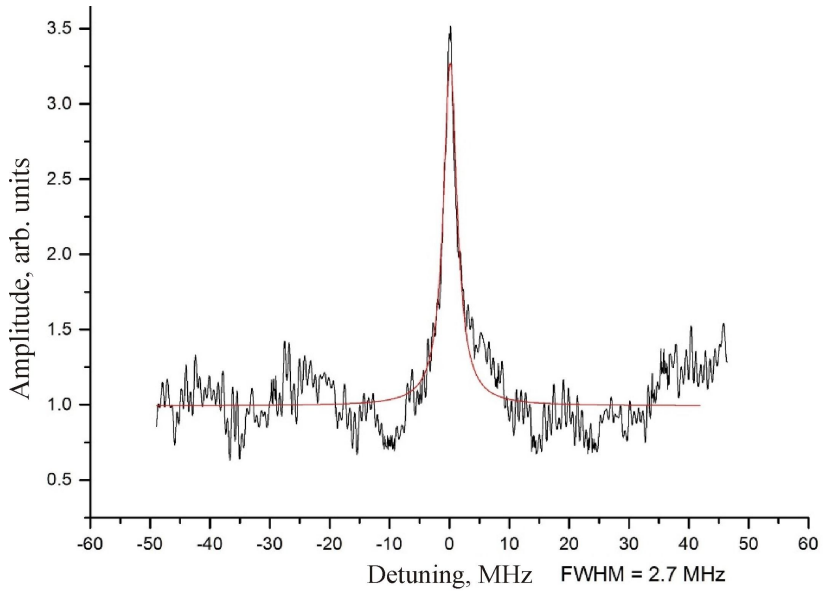

Fig. 5. EIT resonance observed when the coupling beam is scanned around the ^{87}Rb: F = 2 → F' = 2 transition. Lorentzian fit (see red solid line) has the full width at half maximum equal to 2.7 MHz.

to the driver, the diffraction angle also follows this waveform. Changing diffraction angle causes a change in the angle of overlapping between the coupling and probe beams. Moreover, the previous reports [15, 19] have demonstrated a change in the amplitude, a broadening of the EIT width and even destruction of the resonance due to increased angle between the coupling and probe beams. In this situation any high-precision measurements based on this method could become impractical.

Various methods have been used to tackle these problems, e.g. coupling the two beams to a fibre-optic cable [15], where the cable is thought to eliminate the angular change in overlapping of the two beams at the exit. Besides, a double-pass configuration accompanied with a 'cat's eye' optical arraignment have been reported to reduce the beam steering due to changing radio frequency [20]. However, the both methods fail to solve completely the problem because, although the optical fibre eliminates the changes in the overlapping angle, it induces intensity fluctuations due to the triangular waveform. This is because the changes in the diffraction angle change the efficiency of coupling between the optical fibre and the beam. This is a result of the fact that the incident beam moves in and out of focus of the lens positioned at the entrance of fibre launch. This intensity change for the ω_+ beam imposes a fluctuating a.c. Stark shift and, therefore, a variable Rabi frequency. Moreover, the variable power difference between ω_0 and ω_+ also produces a variable shift in the frequency of interaction between the two beams. We have measured this frequency shift to be 1 MHz per a 10 μW power difference between the two beams (see Fig. 6). Finally, any application of the EIT effect based on the AOM becomes impractical, unless the problems mentioned above are completely resolved. This is because one cannot decide whether the changes in the signal are due to the experimental measurements or due to intrinsic spurious effects.

Reduction or complete elimination of the intensity fluctuations and the change in the angle between the ω_0 and ω_+ beams can be carried out with an optical setup that involves a plane-convex lens and a concave mirror. The both optical elements have the same focal length, f = +75 mm. The increased optical path length due to AOM-crystal has been carefully measured and taken into account. As seen from Fig. 7, no intensity fluctuation is detected for the AOM scanning up to 1.6 V. This value implies that the intensity should be stable and the beam can be steered in the

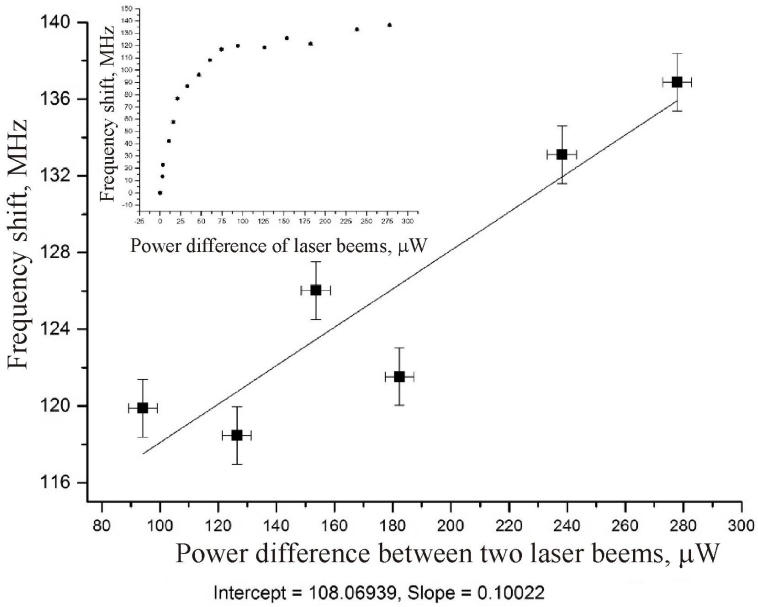

Fig. 6. Shift in the interaction frequency resulting from power difference between the two beams. The inset shows the frequency shift from a 'zero power' when the two beams have equal powers and the interaction-frequency shift is zero. At small power differences, the frequency difference increases rapidly. However, in the EIT regime where the power ratio of the probe and coupling beams is about 1:20, the linear fit is more relevant (see the main panel). It can be seen that the power change resulting from the changes in diffraction efficiency produces a frequency shift. One cannot distinguish between shifts due to power difference and those originated from actual measurements.

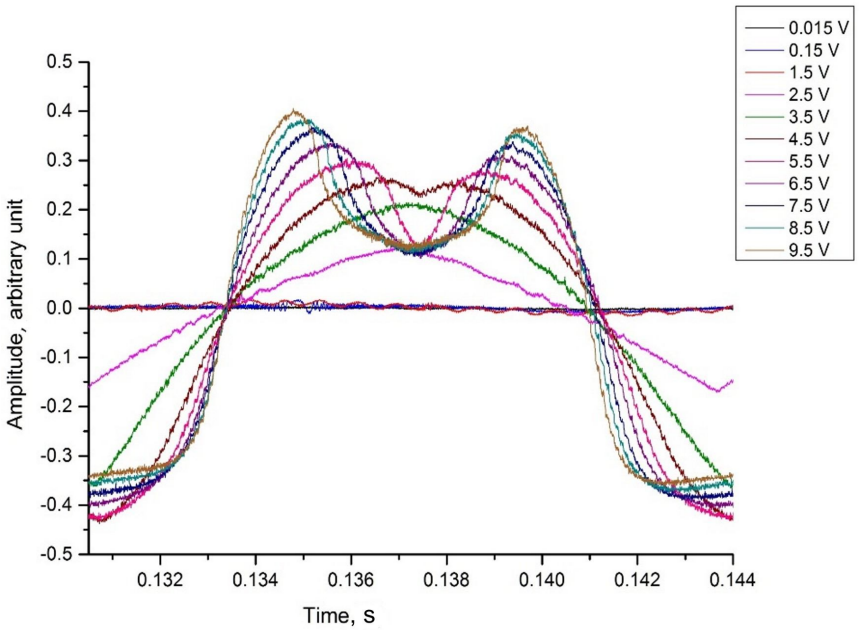

Fig. 7. Intensity change in the ω_+ beam resulting from triangular wave applied. No intensity fluctuation is observed for the scanning voltage lower than 1.5 V. Afterwards, a small change in the intensity is detected and the fluctuations increase rapidly from 2.5 V upward. The triangular waveform can be observed in the intensity profile, especially at V = 2.5 V. Above this value, the intensity profile deviates from the simple triangular waveform, taking on a more complex form. We think this results from the scattering efficiency proportional to $CF \times \cos^2(A_{RF})$, where A denotes the radio-frequency amplitude and CF the coupling factor. To record the intensity changes, a photodiode is placed into the path of retroreflected first-order beam to detect any fluctuations resulting from changing scanning-voltage amplitude applied. Although the time axis is in seconds, in practice we deal with arbitrary units because the 'time' is taken directly from oscilloscope.

modulation range as wide as 33 MHz in the double-pass configuration. Unlike the previous studies, where complex combination of lenses has been used to focus the incident beam on the AOM cell, we instead steer the laser beam directly onto the AOM, with no additional lenses.

The latter experimental scheme is more advantageous because the maximum diffraction efficiency is achieved under the Bragg conditions, whereas both the optical and the acoustic waves are usually thought to be plane waves, which is only an approximation. When a focusing lens is used, outer rays of the input optical beam are not oriented at the same angle as the central part of the beam and, therefore, the beam as a whole is not tilted at the Bragg angle with respect to the acoustic wave front. As a consequence, the outer 'edges' of the beam do not diffract and, hence, are not modulated as efficiently as the central region of the beam. This variation in the diffraction efficiency for different parts of the beam produces an envelope in the modulated frequency of the emergent beam, which results in the beam not having a single modulation parameter. Instead it is spread over a range, which is controlled fundamentally by phonon interaction with the optical wave fronts. The modulation broadening affects ultimately the linewidth of the EIT resonance. Finally, combined implementation of all our experimental devices has offered a significant stability in the degree of overlapping between the beams ω_0 and ω_+ and stable intensity and modulation, when compared with the methods employed previously. This is illustrated by the image of the emergent beam displayed in Fig. 8.

The minimal EIT width that could be measured in our studies amounts to 2.7 MHz. However, this value can be further improved whenever the techniques related to resonance-width reduction are implemented. Examples of these techniques include a use of paraffin-coated cell [21] and a buffer gas added to the interaction cell [20, 21] (except for the effect observed in the Ξ-type interaction, where the buffer gas has been reported to increase the resonance width [24]). Note that the earlier studies have reported the resonance width of up to 20 times smaller than the natural width for D_2 in ^{87}Rb, using a Laguerre−Gaussian coupling beam [25] and an appropriate beam intensity [24, 25].

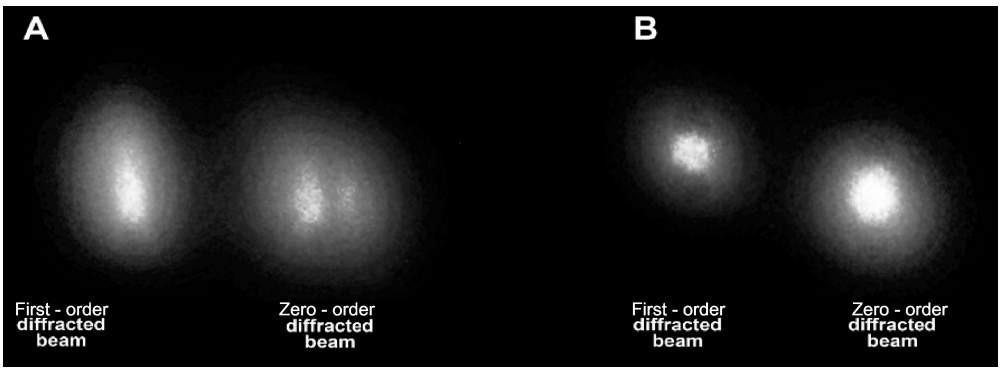

Fig. 8. Image of AOM output showing both zero- and first-order diffracted beams. Panel (A) shows the image taken in case if the AOM cells are set in the double-pass configuration, using a 'cat's eye' optical arraignment. Panel (B) shows the image obtained with the optical arrangement suggested in this work. A difference of the first-order diffracted beams for the two methods is noteworthy; our method has enabled observation of a clear, circular-shaped and smaller-spread beam. A slight change in the vertical position of the first-order diffracted beam seen in panel (B) results from *z*-axis misalignment of the AOM cell, which can be corrected using a three-axis rotational mount.

When all of our 'narrowing' techniques are implemented, the experimental method of ours can be used to build a robust and stable magnetometer using Zeeman sub-levels [26–28]. This can be carried out after our experimental setup is modified via addition of a quarter-wave plate placed

in front of the cell, so that the ω_0 and ω_+ beams are orthogonal and circularly polarized ($\sigma_\pm$). Moreover, an external magnetic field can be applied to the solenoid that houses interaction cell. Then the two beams would interact with different Zeeman sub-levels. Investigations of these points will be a focus of our future work.

5. Conclusions

We have described in detail the experimental setup and the appropriate results obtained for the optimized AOM setup aimed at observing the *V*-type EIT, using the D_1 line of ^{87}Rb. The technical challenges and the intrinsic problems of this method, such as beam-intensity fluctuations and beam-steering effects are thoroughly discussed. The solutions to these problems are formulated in terms of our stable and optimized optical setup. We have shown that the modulation from the AOM is stable and the intensity fluctuations are practically absent for up to 33 MHz. Then the EIT resonance with the linewidth of 2.7 MHz has been observed. This is a result of signal applied externally. We have also demonstrated that our method can produce a sharper, circularly shaped and less spread emergent beam. This is achieved using a simple optical arraignment, when compared with the methods suggested in the earlier works.

The EIT effect based on our method offers several advantages as compared to the other modulation methods. They include production of a bichromatic beam outside of external-cavity diode *laser*, where both the probe and the coupling beams are equally affected by any mechanical or electrical perturbations to the external-cavity diode *laser*. Since the perturbation in this *laser* affects the both beams equally, the mode hopping, beam-power fluctuation and the frequency drift occurring in diode lasers due to temperature effects or misalignments of the cavity are not longer relevant. In fact, these effects are totally eliminated. This fact is important because complicated and expensive temperature and current stabilizations of the external-cavity diode *laser* are then needless. Hence, a cheap diode laser can be used in the optical scheme. Most importantly, unlike the technique of direct modulation of injection current in the laser, the AOM keeps the laser linewidth as small as possible. This is crucial for highly precise measurements.

Acknowledgements

The authors would like to thank the members of Physics Department, University of Leeds, for their collaboration with the University of Sulaimani as a part of split-site PhD program. We are especially thankful to the Experimental Quantum Information group leader and supervisor Ben Varcoe for his helpful discussions. Finally, we are grateful to Rachel Thomson, Matthew Everett, Elizabeth Newton and Freya Wilson for their guidance and numerous discussions.

References

1. Kocharovskaya O, 1992. Amplification and lasing without inversion. Phys. Rep. **219**: 175–190.
2. Hau L V, Harris S E, Dutton Z and Behroozi C H, 1999. Light speed reduction to 17 metres per second in an ultracold atomic gas. Nature. **397**: 594–598.
3. Harris S E and Yamamoto Y, 1998. Photon switching by quantum interference. Phys. Rev. Lett. **81**: 3611–3614.
4. Lukin M D, Yelin S F and Fleischhauer M, 2000. Entanglement of atomic ensembles by trapping correlated photon states. Phys. Rev. Lett. **84**: 4232–4235.
5. Beausoleil R G, Munro W J, Rodrigues D A and Spiller T P, 2005. Applications of electromagnetically induced transparency to quantum information processing. arXiv:quant-

ph/0403028.
6. Scully M O and Fleischhauer M, 1992. High-sensitivity magnetometer based on index-enhanced media. Phys. Rev. Lett. **69**: 1360–1363.
7. Marangos J P, 1998. Topical review: electromagnetically induced transparency. J. Mod. Opt. **45**: 471–503.
8. Fleischhauer M, Imamoglu A and Marangos J P, 2005. Electromagnetically induced transparency: optics in coherent media. Rev. Mod. Phys. **77**: 633–673.
9. Li Y and Xiao M, 1995. Electromagnetically induced transparency in a three-level Lambda-type system in rubidium atoms. Phys. Rev. A. **51**: 2703–2706.
10. Fulton D J, Shepherd S, Moseley R R, Sinclair B D and Dunn M H, 1995. Continuous-wave electromagnetically induced transparency – a comparison of V, Lambda and cascade systems. Phys. Rev. A. **52**: 2302–2311.
11. Gea-Banacloche J, Li Y Q, Jin S Z, and Xiao M, 1995. Electromagnetically induced transparency in ladder-type inhomogeneously broadened media: theory and experiment. Phys. Rev. A. **51**: 576–584.
12. Olson A J and Mayer S K, 2009. Electromagnetically induced transparency in rubidium. Amer. J. Phys. **77**: 116–121.
13. Affolderbach C, Knappe S, Wynands R, Taĭchenachev A and Yudin V, 2002. Electromagnetically induced transparency and absorption in a standing wave. Phys. Rev. A. **65**: 1–10.
14. Cox K, Yudin V I, Taichenachev A V, Novikova I and Mikhailov E E, 2011. Measurements of the magnetic field vector using multiple electromagnetically induced transparency resonances in Rb vapor. Phys. Rev. A. **83**: 2–5.
15. Akulshin A, Barreiro S and Lezama A, 1998. Electromagnetically induced absorption and transparency due to resonant two-field excitation of quasidegenerate levels in Rb vapor. Phys. Rev. A. **57**: 2996–3002.
16. Scully M and Zubairy M S. Quantum optics. Cambridge: Cambridge University Press (2001).
17. Gordon E I, 1966. A review of acoustooptical deflection and modulation devices. Proc. IEEE. **54**: 1391–1401.
18. Steck D A, 2010. Rubidium 87 D line data. http//steck.us/alkalidata.
19. Carvalho P R S, De Araujo L E E and Tabosa J W R, 2004. Angular dependence of an electromagnetically induced transparency resonance in a Doppler-broadened atomic vapor 063818. Phys. Rev. A. **70**: 1–5.
20. Donley E A, Heavner T P, Levi F, Tataw M O and Jefferts S R, 2005. Double-pass acousto-optic modulator system. Rev. Sci. Instrum. **76**: 3–8.
21. Klein M, Hohensee M, Phillips D F and Walsworth R L, 2011. Electromagnetically induced transparency in paraffin-coated vapor cells. Phys. Rev. A. 83: 1–10.
22. Brandt S, Nagel A, Wynands R and Meschede D, 1997. Buffer-gas-induced linewidth reduction of coherent dark resonances to below 50 Hz. Phys. Rev. A. **56**: R1063–R1066.
23. Erhard M and Helm H, 2001. Buffer-gas effects on dark resonances: theory and experiment. Phys. Rev. A. **63**: 1–13.
24. Sargsyan A, Sarkisyan D, Krohn U, Keaveney J and Adams C, 2010. Effect of buffer gas on an electromagnetically induced transparency in a ladder system using thermal rubidium vapor. Phys. Rev. A. **82**: 2–5.
25. Ranjita Chanu S and Natarajan V, 2013. Narrowing of resonances in electromagnetically

induced transparency and absorption using a Laguerre–Gaussian control beam. Opt. Commun. **295**: 150–154.

26. Javan A, Kocharovskaya O, Lee H and Scully M, 2002. Narrowing of electromagnetically induced transparency resonance in a Doppler-broadened medium. Phys. Rev. A. **66**: 13805.
27. Dimitrijevic J, Arsenovic D and Jelenkovic B M, 2007. Intensity dependence narrowing of electromagnetically induced absorption in a Doppler-broadened medium. Phys. Rev. A. **76**: 1–7.
28. Yudin V I, Taichenachev A V, Dudin Y O, Velichansky V L, Zibrov A S and Zibrov S A, 2010. Vector magnetometry based on electromagnetically induced transparency in linearly polarized light. Phys. Rev. A. **82**: 1–7.
29. Katsoprinakis G, Petrosyan D and Kominis I K, 2006. High frequency atomic magnetometer by use of electromagnetically induced transparency. Phys. Rev. Lett. **97**: 1–4.

Dastan Khalid and Hawri O. Majeed. 2017. Optimized acousto-optic modulation for the *V*-type electromagnetically induced transparency in rubidium-87 D_1 line. Ukr.J.Phys.Opt. **18**: 168 – 178.

Анотація. *Представлено експериментальну установку оптимізованого акустооптичного модулятора, призначеного для спостереження електромагнітно індукованого резонансу прозорості V-типу на лінії D_1 рубідію-87, де повна ширина на половині максимуму дорівнює 2,7 МГц. Докладно обговорено можливі артефакти та небажані впливи на сигнал, що з'являються в рамках нашого методу. Рішення таких технічних проблем, як відхилення променя та коливання інтенсивності, знайдено в оптимізації оптичної установки. Зазначений спосіб пропонує низку переваг, зокрема єдиний діодний лазер із зовнішнім резонатором для створення біхроматичного оптичного поля поза лазером, завдяки чому і взаємодіючий, і зондовий промені мають однакові властивості. Більше того, збурення лазера через навколишні впливи однаково впливають на обидва пучки. Так можна виключити впливи модових перескоків, флуктуацій потужності променя та дрейфу частоти на резонанс. Тоді немає потреби в складній і дорогій стабілізації температури та струму, а також в блокувальному блоці. Простота та стабільність вдосконаленого устаткування робить наш метод придатним для багатьох застосувань, заснованих на електромагнітно індукованій прозорості, особливо тих, що стосуються області точних вимірювань.*